(12)

FG.

Office of Naval Research

Contract N00014-76-C-0060 NR 064-478

Technical Report No. 27

DYNAMIC STRESS INTENSITY FACTOR OF HOMALITE-100

by

A.S. Kobayashi and S. Mall

December 1976

The research reported in this technical report was made possible through support extended to the Department of Mechanical Engineering, University of Washington, by the Office of Naval Research under Contract N00014-76-C-0060 NR 064-478. Reproduction in whole or in part is permitted for any purpose of the United States Government.

Department of Mechanical Engineering
College of Engineering
University of Washington

DYNAMIC STRESS INTENSITY FACTOR OF HOMALITE-100

by

A. S. Kobayashi and S. Mall
University of Washington
Department of Mechanical Engineering

ABSTRACT

Dynamic stress intensity factors of Homalite-100 determined by T. Kobayashi and Dally are compared with those previously obtained by the authors where similarities in the two results for single-edged notch specimens of various configurations are noted. Dynamic stress intensity factors of Araldite B obtained by Kalthoff, Beinert and Winkler and those of Homalite-100 obtained by the authors are then compared and again similarities in the two results and in particular the scatters in experimental data for wedge-loaded DCB specimens of different sizes are noted. All three teams of investigators used static near-field solution to compute the dynamic stress intensity factors from recorded dynamic isochromatics or dynamic caustics. Errors generated through this use of static near-field solutions as well as through the use of larger isochromatic lobes are thus discussed.

INTRODUCTION

For the past several years the writers and their colleagues have been using dynamic photoelasticity to determine the dynamic stress intensity factors*, K_D, and crack velocities of propagating cracks in unstiffened and stiffened single-edged notch tension plates under fixed grip loading with and without impact conditions [1,2], dynamic tear test (DTT) specimens [3], and wedge-loaded double cantilever beam (DCB) specimens [4]. In all these studies, a static near field solution was used to compute the dynamic stress intensity factor from the

---

* Dynamic stress intensity factor of a running crack in a particular material is often referred to as the dynamic fracture toughness or the dynamic fracture resistance of the material.

dynamic isochromatic patterns surrounding the running crack following Irwin's procedure of 1958 [5]. More recently T. Kobayashi and Dally have used dynamic photoelasticity to determine dynamic stress intensity factors of propagating cracks in various birefringent polymers [6,7]. Also Kalthoff et al. have, through the use of caustics, determined the dynamic stress intensity factors of Araldite B using wedge-loaded DCB specimens [8]. The results obtained by these three independent teams of researchers, at first, appeared to be mutually contradictory to the extent that some results are quoted out of context to support a particular fracture dynamic and crack arrest criteria against others [9]. The purpose of this paper is to identify some of the common results obtained among these three teams of investigators and to analyze the possible causes which led to these apparent discrepancies.

DYNAMIC STRESS INTENSITY FACTOR

In the three investigations quoted above, a static near-field state of stress was fitted to either the dynamic isochromatics or the dynamic caustics surrounding a running crack and the static stress intensity factor thus obtained was considered to be the dynamic stress intensity factor, K_D. Ignoring for the time being the inherent as well as additional possible sources of errors involved in this data reduction scheme, the dynamic stress intensity factor, as defined by the static near-field solution, versus crack velocity relation can be plotted in a nondimensional format in order to reduce as much as possible the effects of material variabilities between the three investigators. Figure 1 shows the nondimensionalized crack velocity versus nondimensionalized dynamic stress intensity factor relation obtained from the dynamic photoelastic data in Homalite-100 plate, 9.5mm (3/8 in.) in thickness, by Bradley who used 254mmx254mm (10in.x10in.) single-edged notch plates loaded under fixed grip condition. Most of the data scatter in Figure 1 is mainly due to inaccurate crack velocity measurements which were calculated directly from the

crack tip position versus time data and is also due in part to the stress wave effects. T. Kobayashi and Dally [7], on the other hand, used smoothed crack tip position versus time curves for crack velocity calculations and observed no stress wave effects. The uniform crack velocity thus obtained from the smoothed crack length versus time curve is consistent with the uniform crack velocities observed in fracturing glass using ultrasonic-ripple marking technique [11] and in polymethylmethacrylate using streak photography [12]. By compressing our scatters in crack velocities, we too can obtain a better correlation between dynamic stress intensity factor and crack velocity as shown in Figure 2.

The dynamic stress intensity factor versus crack velocity relation by T. Kobayashi and Dally [7] for 19.05mm thick Homalite-100 plates was converted to nondimensionalized dynamic stress intensity factor versus nondimensionalized crack velocity relation and is also plotted in Figure 2. Despite the scatter in our data, the two nondimensionalized stress intensity factors at the lower crack velocities agree well, particularly when one considers the differences in the material properties of the Homalite-100 plates of different thicknesses and of different fabrication periods. The static fracture toughnesses of the two different Homalite-100 plates differed by approximately 30 percent and the estimated differences between the nondimensionalized averaged dynamic stress intensity factor at crack arrest was about 12 percent.

Although one can construct an averaged dynamic stress intensity factor versus crack velocity relation, which assumes the familiar Γ-shaped curve [13], through the scattered experimental data in Figure 2, we are reluctant to establish such definitive dynamic fracture characterization in view of our recent experiences with dynamic finite element analysis of a fracturing tapered DCB specimen [14] and dynamic finite difference analyses of fracturing pipes [15]. The results of these numerical analyses indicate that an elastic crack must run at intermittent crack

velocities in order for a smoothly varying dynamic stress intensity factor versus crack velocity relation to exist as a material property. Alternatively, the dynamic stress intensity factor must vary intermittently in order to maintain smoothly varying crack velocities and thus precludes a unique Γ-shaped crack velocity versus dynamic stress intensity factor relation. At the present stage of development, in the writers' opinion, neither dynamic photoelasticity nor dynamic caustics can provide accurate dynamic stress intensity factor nor crack velocity to resolve this controversy. In fact, the available little data on relatively accurate crack velocity measurements indicate that the crack velocity does vary uniformly at least in glass [11] and in polymethylmethacrylate [12] thus leaving us with the only alternatives of nonunique relation between dynamic stress intensity factor and crack velocity if the above mentioned numerical analyses had correctly modeled dynamic fracture.

Figure 2 also shows another point of departure between our results and those of T. Kobayashi et al. who observed complete crack branching at $K_D/K_{IC} = 3.7$ [7], where we could not relate crack branching with any instantaneous dynamic stress intensity factor. Perhaps this difference in crack-branching dynamic stress intensity factor also involves the definition of crack branching. Our fractured Homalite-100 specimens showed many minute crack branches prior to the onset of major crack branching.* Obviously considerable unaccountable fracture energy was dissipated through these minor crack branches which could have resulted in our indecisive crack-branching dynamic stress intensity factors. In addition, the close proximity of the two running cracks, which just branched, accentuates the interchange between the dynamic energy released and the kinetic energy surrounding the crack tip [17] and thus the static near-field solution can no longer be used for calculating the dynamic stress intensity factor of a bifurcated or trifurcated crack surrounded by a single dynamic isochromatic lobe. Lacking a proper data

* See for example Figures 2 and 3 in Reference [16].

reduction procedure, a gross energetic approach was used to arrive at an empirical crack branching criterion. An average dynamic energy release rate, which is defined as the total dynamic energy released divided by the total crack surface, was computed by using the single-crack tip near field solution but by incorporating all measurable major and minor crack surfaces. This average dynamic energy release rate, $\mathcal{G}_D]_{ave}$, which incorporates the gross effect of kinetic energy feedback in driving the crack, was found to be of 2.1 - 2.7 times the static critical strain energy release rate, $\mathcal{G}_{IC}$ [16]. This crudely estimated crack branching $\mathcal{G}_D]_{ave}$ indicates that branching will occur when sufficient energy is available to propagate two separate cracks. Obviously, further refinements of such data reduction procedure are necessary before a crack branching criterion can be established.

Our preference for plotting the dynamic energy release rate instead of the more directly calculable dynamic stress intensity factor from the dynamic isochromatics and dynamic caustic as per T. Kobayashi et al. [7], and Kalthoff et al. [8], respectively, can also be attributed to the fact that the total sum of dynamic energy release rate during crack propagation can be related to the total kinetic energy and potential energy in the test specimen at each instant of time thus providing one with an accuracy assessment based on first principles. Computation of this dynamic energy released, $\mathcal{G}_D$, from dynamic stress intensity factor, K_D, was accomplished by Freund's formula [23] using the measured crack velocity. The generality of this part of Freund's solution was discussed by Nilsson [25].

Figure 3 shows a comparison between the dynamic stress intensity factor versus smoothed crack velocities in wedge-loaded DCB specimens of Araldite B [8] and Homalite-100 [4]. Here again, the smoothed crack length-versus-time curves was used to eliminate the many oscillations in crack velocities thus making it similar in shape to Kalthoff's curve. Although no direct correlation between the two "Γ"

curves are possible due to differences in material properties between Araldite B and Homalite-100, it is interesting to note that scatters, which were appreciably larger than those of T. Kobayashi et al., in data points of these two materials are very similar in these nondimensionalized plots. This scatter could be due to the larger interaction between kinetic energy and dynamic energy released in our smaller DCB specimens in contrast to the large monolithic single-edged notch specimens used by T. Kobayashi and Dally. An up-to-date detailed discussion on the high dynamic amplification factor due to this intense interchange between kinetic energy and dynamic energy released through crack propagation in wedge-loaded DCB specimen can be found in Reference [18].

It is interesting to note that in Kalthoff's experiment, the dynamic stress intensity factor oscillated after crack arrest, eventually converging to the static stress intensity factor at crack arrest, K_{Ia}, which gradually decreased with increasing arrest crack length. This gradual decrease in K_{Ia} with higher driving force of K_{IQ} is in accord with the belief that the static stress intensity factor at crack arrest is not a material property [10,17].

The above comparison of experimental results shows that although the results obtained by the three teams are in qualitative agreement with each other, data scatter in Kalthoff's and our experiments were consistently larger than those of T. Kobayashi and Dally. It thus appeared appropriate to reassess our data reduction scheme at this time in search of the cause or causes of the data scatter in Kalthoff and our results. As mentioned previously, the static near field solution was used by all to reduce their dynamic optical data. Kalthoff et al. and we used the optical data within a radial distance of $r = 2.5 \sim 5$mm (0.1 ~ 0.2 inch) region surrounding the moving crack tip while T. Kobayashi et al. in some of their data reduction schemes considered regions as large as $r \doteq 25.4$mm (1 inch)[19]. The possible numerical errors involved in using larger crack tip region in a uniform

dynamic stress field surrounding a Yoffe crack [20] was discussed previously [10]. Since this error analysis did not incorporate the effect of nonuniform dynamic stress field, such error analysis is considered in the following section.

NEAR-FIELD ELASTO-DYNAMIC STATE

The near-field elasto-dynamic state of stresses for a crack propagating at a constant velocity, c, is [21]

$$\sigma_{xx} = a_1 \frac{3}{2} \{(2 s_1^2 - s_2^2 + 1) r_1^{-1/2} \cos \frac{\theta_1}{2} - \frac{4 s_1 s_2}{(1+s_2^2)} r_2^{-1/2} \cos \frac{\theta_2}{2}\}$$

$$+ a_2 8(s_1^2 - s_2^2) + a_3 \frac{15}{2} \{(2 s_1^2 - s_2^2 + 1) r_1^{1/2} \cos \frac{\theta_1}{2}$$

$$- \frac{4 s_1 s_2}{(1+s_2^2)} r_2^{1/2} \cos \frac{\theta_2}{2}\} + \ldots \qquad (1a)$$

$$\sigma_{yy} = a_1 \frac{3}{2} \{- (1+s_2^2) r_1^{-1/2} \cos \frac{\theta_1}{2} + \frac{4 s_1 s_2}{(1+s_2^2)} r_2^{-1/2} \cos \frac{\theta_2}{2}\}$$

$$+ a_3 \frac{15}{2} \{- (1+ s_2^2) r_1^{1/2} \cos \frac{\theta_1}{2} + \frac{4 s_1 s_2}{1+s_2^2} r_2^{1/2} \cos \frac{\theta_2}{2}\} + \ldots \qquad (1b)$$

$$\tau_{xy} = a_1 3 s_1 \{r_1^{-1/2} \sin \frac{\theta_1}{2} - r_2^{-1/2} \sin \frac{\theta_2}{2}\} + a_3 15 s_1 \{- r_1^{1/2} \sin \frac{\theta_1}{2}$$

$$+ r_2^{1/2} \sin \frac{\theta_2}{2}\} + \ldots$$

where

$$s_1^2 = 1 - c^2/c_1^2 \qquad \text{and} \qquad s_2 = 1 - c^2/c_2^2 \qquad (2a)$$

$$r_1^2 = x^2 + s_1^2 y^2 \qquad \text{and} \qquad r_2^2 = x^2 + s_2^2 y^2 \qquad (2b)$$

$$\tan\theta_1 = \frac{s_1 y}{x} \qquad \text{and} \qquad \tan\theta_2 = \frac{s_2 y}{x} \qquad (2c)$$

c, c_1 and c_2 are the crack velocity, dilatational wave velocity and distortional wave velocity, respectively.

x and y are moving rectangular coordinates with origins at the propagating crack tip.

The above near-field state represents the first three terms in Reference [21] and was selected for comparison with the three parameter representations in Reference [19]. It can be easily shown that for zero crack velocity or $c \to 0$, Equations [1] reduce to those in Reference [22]. The arbitrary constant coefficient, a_1, can also be represented in terms of the more familiar dynamic stress intensity factor as

$$a_1 = \frac{K_D}{2\sqrt{2\pi}} \frac{4(1+s_2^2)}{3[4s_1s_2 - (1+s_2^2)^2]} \tag{3}$$

where K_D is the dynamic stress intensity factor after Freund [23] and reduces to the static stress intensity factor, K, when $c \to 0$. It can also be shown that $a_2 \to -\sigma_{ox}/[8(s_1^2 - s_2^2)]$ when $c \to 0$ where σ_{ox} is the often-quoted remote stress component [5,7].

The dynamic isochromatic fringe loop can be represented by the well-known formula of

$$\tau_{max} = [(\sigma_{xx} - \sigma_{yy})^2/4 + \tau_{xy}^2]^{1/2} \tag{4}$$

The diameter of caustics, $\bar{w}$, on the other hand [24], is

$$\bar{w} = -z_o t f \, \text{grad}(\sigma_{xx} + \sigma_{yy}) \tag{5}$$

where z_o, t and f are the distance between the midplane of the specimen and screen, thickness of the specimen and the optic constant of the specimen, respectively. In the following, Equations (1), (4) or (5) will be used to establish the theoretical dynamic isochromatics or dynamic caustics for a known dynamic stress intensity factor which will be compared with the stress intensity factor computed by using the static near-field solutions.

Dynamic Isochromatics

Unlike the Yoffe crack [20], the near-field solution of Equations (1) and (2) show that the dynamic stress intensity factor will not approach that of the static stress intensity factor, K, as $r = \sqrt{x^2 + y^2} \to 0$. The exact deviation between dynamic and static stress intensity factors, K and K_D, for a given crack velocity, c, varies with the procedure in which static near field state of stress is fitted to the dynamic near field state of stress. For example, if a two-parameter static isochromatic lobe is matched with a one-parameter dynamic isochromatic lobe at the maximum radial distance, r_{max}, in Fig. 2 of Reference [1], then $K/K_D = 1.02$ and 1.07 for $c/c_1 = 0.106$ and 0.159, respectively. Such inherent error in K_D estimation is thus negligible at lower crack velocities of $c/c_1 < 0.1$ where much of the crack arrest stress intensity factor, K_a, is inferred, but otherwise is unavoidable regardless of the smallness of the near field region concerned.

Having established the inherent error in the use of the static state of stress for K_D estimation, we then posed the question of what additional errors if any are involved by evaluating the dynamic optical data in a larger region. For this purpose, the three-parameter representation of the dynamic near field solution as shown by Equation (1) was used to model a crack propagating at constant velocities of $c/c_1 = 0.00001$, 0.05 and 0.15. The dynamic state corresponding to $c/c_1 = 0.00001$ was used as the corresponding static solution after verifying the negligible discrepancy between the static and dynamic state of this extremely low crack velocity. Dynamic modulus $E = 4.65$ GPa (675 ksi) and Poisson's ratio $\nu = 0.345$ for Homalite-100 were used to simulate the actual test conditions in dynamic photoelasticity.

Typical dynamic states surrounding the crack tip propagating at the constant velocity, where $K_D/K_{IC} = 2$, and 0.8 for $c/c_1 = 0.15$ and 0.05, respectively, were then

considered. Isochromatic fringes which pass through references points were then plotted for $K_D/K_{IC} = 2.2$, 2.0 and 1.8 at $c/c_1 = 0.15$ and 0.00001 as shown in Figures 4 and 5. The smaller static isochromatic lobe of $c/c_1 = 0.00001$ in these figures indicates that an inherent overestimation of 24% in K_D is involved if the static isochromatic lobe is only stretched to match r_{max} of the dynamic isochromatic lobe in Figure 4. Likewise K_D will be overestimated by 12 percent if the smaller dynamic isochromatics in Figure 5 are considered. This increased error due to increased size in isochromatics indicates the importance of a dynamic analysis when larger isochromatic lobes are considered and is in qualitative agreement with the error analysis in Reference [10] where the artificial Yoffee crack [20] was used to estimate the size effect in the backward tilting isochromatic lobes. Within a sufficiently close region surrounding the running crack tip and in the absence of any parasitic stress waves, the magnitude of this overestimation will be reduced but the statistically computed stress intensity factor will always be larger than the actual dynamic value.

Figure 4 also indicates the relative insensitivity of the size of larger isochromatic lobe to a $\pm$ 10 percent change in dynamic and static stress intensity factors. Dimensional changes with small changes in stress intensity factors are accomplished mainly by the small changes in the tilting of the isochromatic lobe, θ_{max}, verifying the original conclusion by Bradley [1]. Such insensitivity to K_D raises the possibility that the small oscillations in dynamic stress intensity factor could be masked by the average dynamic stress intensity factor of larger isochromatic lobes unless the data reduction procedure is sensitive to θ_{max} change.

The above numerical examples reconfirmed our suspicion that considerable error may be induced when the static near-field solution is used to compute the dynamic

stress intensity factor using relatively large isochromatics. The use of higher order terms in the static eigen-function expansion formula may not improve the accuracy in the data reduction procedure but could increase the error involved.

Figure 6 shows the larger dynamic isochromatic lobes at crack velocities of $c/c_1 = 0.05$. Static isochromatic lobes were not included in Figure 6 since these static isochromatics were at the most only 2-3 percent smaller in radial distances than the corresponding dynamic isochromatics. Likewise coincidence existed in the smaller isochromatics. Error analysis of our data reduction procedure at this crack velocity is of particular interest since small differences in the dynamic stress intensity factors, K_D, at this portion of the Γ-curve could result in different crack arrest stress intensity factor, K_a, which is often estimated by extrapolating the lower end of the Γ-curve at $c/c_1 = 0$. Figure 6 shows that for slower crack velocities of $c/c_1 = 0.05$, the static near-field isochromatics is a reasonable representation of the dynamic state. Data scatter in the lower end of the Γ-curve could be due to either experimental errors or the actual fluctutations in K_D.

As another assessment of possible error involved in using larger isochromatic lobes, a constant velocity crack of $c/c_1 = 0.15$ running into a constant and linearly varying static stress fields of $\sigma_{yy} = 0.689$ MPa (100 psi) at $y \neq 0$ and $0.689 \cdot y$ MPa ($100 \cdot y$ psi), respectively, were considered. Such stress fields simulate two types of reflected tension waves impacting the constant velocity crack and represent the dynamic near-field solution immediately prior to the elevation in dynamic stress intensity factor due to the impinging tensile waves. The magnitude as well as the gradient of these impinging tensile wave fronts were taken from the experimental values of transient waves in Reference 26. Figures 7 and 8 show the two levels of near-field isochromatics with the superimposed $\sigma_{yy} = 0.689$ MPa (100 psi) and $0.689 \cdot y$ MPa ($100 \cdot y$ psi), respectively. Also shown in Figures 7 and 8 are the dynamic near-field isochromatics without the superimposed static states of stress. It is immediately obvious that the larger dynamic isochromatics are significantly altered

by the superimposed moderate tensile field. In terms of the data reduction procedure, the larger isochromatics will predict a significantly higher apparent dynamic stress intensity factor while the smaller isochromatic lobes which are dominated by the dynamic singular stress field will predict more accurately the instantaneous dynamic stress intensity factor.

Dynamic Caustics

The dynamic near-field region considered by Equation 5 relates to a region of $r_{max} \doteq 0.1$ inch [8]. Thus the inherent error as well as the possible error involved in predicting dynamic stress intensity factors in the presence of an impinging stress wave follow those involved in the smaller isochromatic lobes discussed previously. The qualitative agreement in data scatter in Figure 3 and the observed oscillation in dynamic stress intensity factors could be explained by the similarity in Kalthoff's and our data reduction procedures which are confined to the smaller near field surrounding the running crack.

CONCLUSIONS

1. Qualitative agreements between the dynamic stress intensity factors of Homalite-100 plates obtained by T. Kobayashi et al. and the wedge-loaded DCB results for Araldite B by Kalthoff et al. and the authors' old results are observed.
2. Differences in the various results obtained by the three teams of investigators could be attributed in part to the accuracy and interpretation of crack velocity data.
3. The use of static near-field stresses in place of the dynamic near-field stresses in computing the dynamic stress intensity factors could result in overestimation of these values at the higher crack velocity of $c/c_1 = 0.15$.

4. An impinging stress wave on a moving crack could significantly change the shape of the isochromatics and thus introduce substantial error in the computed stress intensity factor.
5. If the static stress field must be used in evaluating the dynamic photoelasticity results at higher crack velocities or in the presence of parasitic stress waves, the dynamic stress intensity factors should be computed by using the smallest isochromatics, preferably within 2.5mm (0.1 inch) distance of the crack tip at higher crack velocities.

ACKNOWLEDGEMENT

The results of this investigation were obtained in a research contract funded by the Office of Naval Research under Contract No. N000014-76-C-0060, NR 064-478. The authors wish to acknowledge the support and encouragement of Drs. N.R. Perrone and D. Mulville of ONR.

REFERENCES

1. Kobayashi, A.S., Wade, B.G. and Bradley, W.B., "Fracture Dynamics of Homalite-100", Deformation and Fracture of High Polymers (edited by H.H. Kausch, J.A. Hassell, and R.I. Jaffee), Plenum Press, New York, 1973, pp. 487-500.

2. Wade, B.G. and Kobayashi, A.S., "Photoelastic Investigation on the Crack-Arrest Capability of Pretensioned Stiffened Plate", Experimental Mechanics, Vol. 15, No. 1, January 1975, pp. 1-9.

3. Kobayashi, A.S. and Chan, C.F., "A Dynamic Photoelastic Analysis of Dynamic Tear Test Specimen", Experimental Mechanics, Vol. 16, No. 5, May 1976, pp. 176-181.

4. Kobayashi, A.S., Mall, S. and Lee, M.H., "Fracture Dynamics of Wedge-Loaded DCB Specimen", Cracks and Fracture, ASTM STP 601, 1976, pp. 274-290.

5. Irwin, G.R., "Discussion and Authors' Closure of the Paper, The Dynamic Stress Distribution Surrounding a Running Crack - A Photoelastic Analysis", Proc. of SESA, XVI (1), 1958, pp. 93-96.

6. Kobayashi, T. and Fourney, W.L., "Dynamic Photoelastic Investigations of Crack Propagation", Proc. of 12th Annual Meeting of the Society of Engineering Sciences, Univ. of Texas at Austin, Oct. 20-22, 1975, pp. 131-140.

7. Kobayashi, T. and Dally, J.W., "The Relation Between Crack Velocity and Stress Intensity Factor in Birefringent Polymers", to be published in Proc. of E-24 Symposium on Fast Fracture and Crack Arrest, ASTM STP 1977.

8. Kalthoff, J.F., Beinert, J. and Winkler, S., "Dynamic Stress Intensity Factors for Arresting Cracks in DCB Specimens", ibid loc cit.

9. Crosley, R.P. and Ripling, E.J., "Characteristics of a Run-Arrest Segment of Crack Arrest", ibid loc cit.

10. Kobayashi, A.S., Emery, A.F. and Mall, S., "Dynamic Finite Element and Dynamic Photoelastic Analyses of Crack Arrest in Homalite-100 Plates", ibid loc cit.

11. Döll, W., "Investigation of the Crack Branching Energy", International Journal of Fracture, Vol. 11, 1974, pp. 184-186.

12. Bergkvist, H., "Some Experiments on Crack Motion and Arrest in Polymethylanethacrylate", Eng. Fracture Mechanics, Vol. 6, 1974, pp. 621-626.

13. Irwin, G.R., "Comments on Dynamic Fracture Testing", Proc. of the Int. Conf. on Dynamic Fracture Toughness, The Welding Institute, July 1976, pp. 1-9.

14. Urabe, Y., Kobayashi, A.S., Emery, A.F. and Love, W.J., "Dynamic Finite Element Analysis of a Tapered DCB Specimen", to be published in the Proc. of the International Conference on Fracture Mechanics and Technology, Hong Kong, March 21-25, 1977.

15. Emery, A.F., Love, W.J. and Kobayashi, A.S., "Influence of Dynamic Fracture Toughness on Elastic Crack Propagation in a Pressurized Pipe", ibid loc cit.

16. Kobayashi, A.S., Mall, S. and Bradley, W.B., "Dynamic Photoelastic Analysis of Crack Branching", Proc. of 12th Annual Meeting of Society of Engineering Science, The University of Texas at Austin, Oct. 20-22, 1975, pp. 1005-1014.

17. Hahn, G., Gehlen, R.C., Hoagland, R.G., Kanninen, M.F., Popelar, C. and Rosenfield, A.B., "Critical Experiments, Measurements and Analyses to Establish a Crack Arrest Methodology for Nuclear Pressure Vessel Steels", 4th Quarterly Progress Report, Task 62, Battelle Columbus Laboratories BMI-1939, Nov. 1975.

18. Kanninen, M.F., Mills, E., Hahn, G.T., Marshall, C., Borek, D., Cogle, A., Masubuchi, K. and Itoga, K., "A Study of Ship Hull Crack Arrester Systems", Battelle Columbus Laboratories, report prepared under Contract N00024-75-C-4325, Dec. 18, 1975.

19. Irwin, G.R., Dally, J.W., Kobayashi, T. and Etheridge, J.M., "A Dynamic Photoelastic Study of the Dynamic Fracture Behavior of Homalite-100", NUREG-75/107, US NRC, Sept. 1975.

20. Yoffe, E.H., "The Moving Griffith Crack", Philosophical Magazine, Vol. 42, 1951, pp. 739-750.

21. King, W.W., Malluck, J.F., Aberson, J.A. and Anderson, J.M., "Finite Element Simulation of a Rapidly Propagating Crack", to be published in Proc. of E-24 Symposium on Fast Fracture and Crack Arrest, ASTM STP, 1977.

22. Williams, M.L., "On the Stress Distribution at the Base of a Stationary Crack", Journal of Applied Mechanics, Vol. 24, No. 2, Trans. of ASME, 1957, pp. 109-114.

23. Freund, L.B., "Crack Propagation in an Elastic Solid Subjected to General Loading-I, Constant Rate of Extension", J. of the Mech. and Phys. of Solids, Vol. 20, 1972, pp. 129-140.

24. Theocaris, P.S., "Local Yielding Around a Crack Tip in Plexiglass", J. of Applied Mechanics, Trans. of ASME, Vol. 37, Series E, No. 2, June 1970, pp. 409-415.

25. Nilsson, F., "A Note on the Stress Singularity at a Non-Uniformly Moving Crack Tip", J. of Elasticity, Vol. 4, 1974, pp. 73-75.

26. Kobayashi, A.S., and Wade, B.G., "Crack Propagation and Arrest in Impacted Plates", Proc. of an International Conf. on Dynamic Crack Propagation, edited by G.C. Sih, Noordhoff Int. Pub., Leyden, 1974, pp. 663-677.

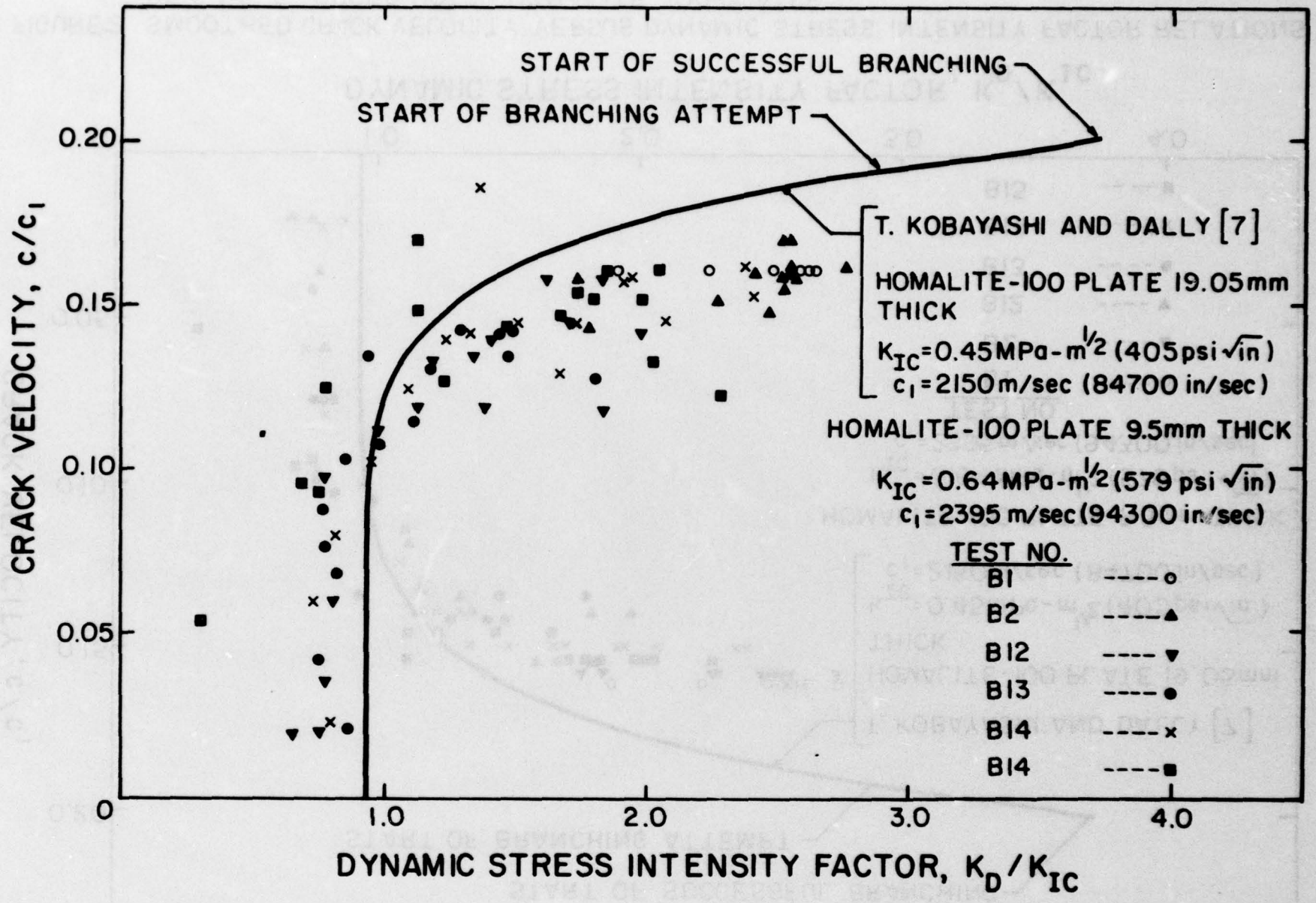

FIGURE 1. SMOOTHED CRACK VELOCITY VERSUS DYNAMIC STRESS INTENSITY FACTOR RELATIONS OF SINGLE-EDGED NOTCH HOMALITE-100 PLATES.

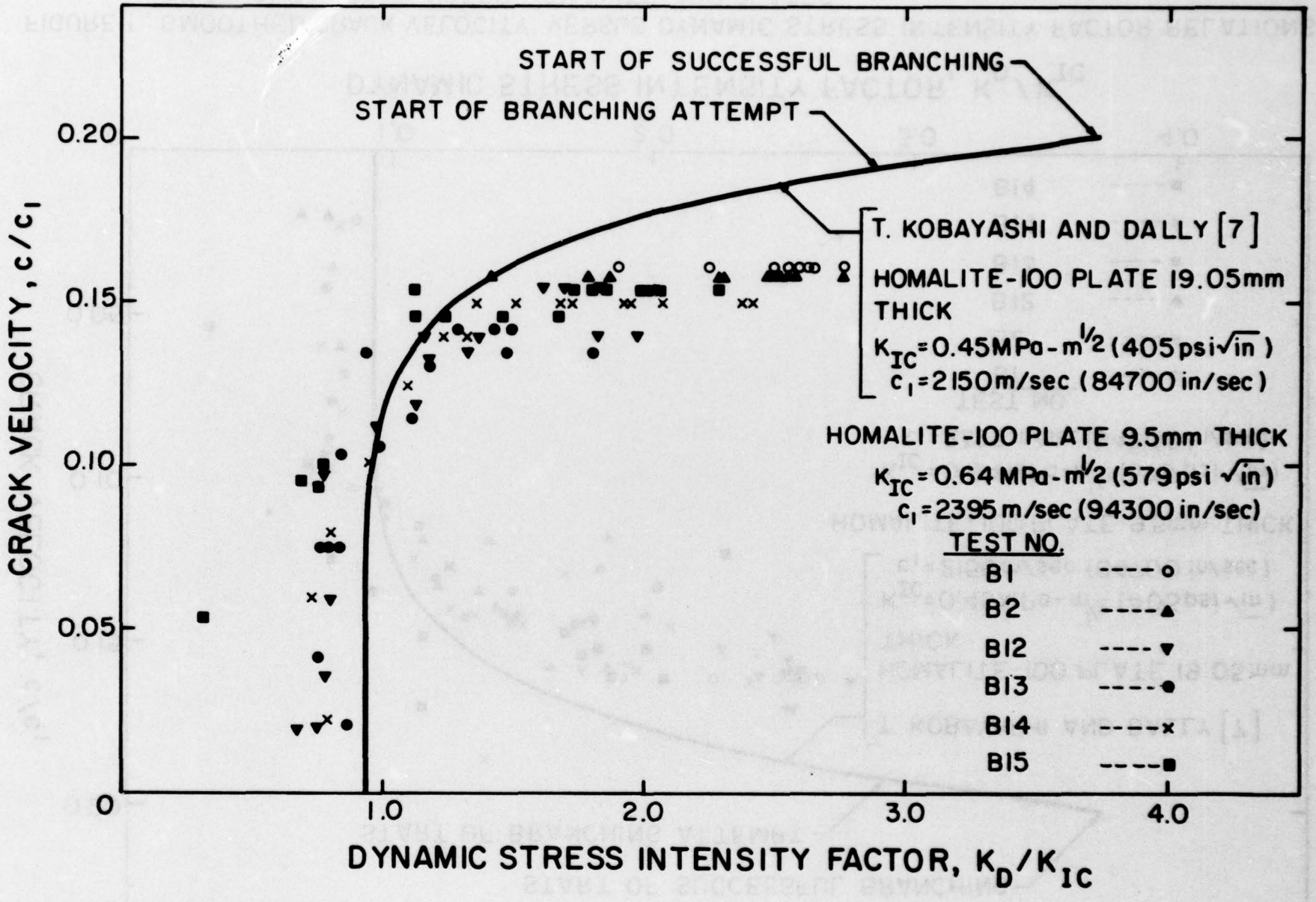

FIGURE 2. SMOOTHED CRACK VELOCITY VERSUS DYNAMIC STRESS INTENSITY FACTOR RELATIONS OF SINGLE-EDGED NOTCH HOMALITE-100 PLATES.

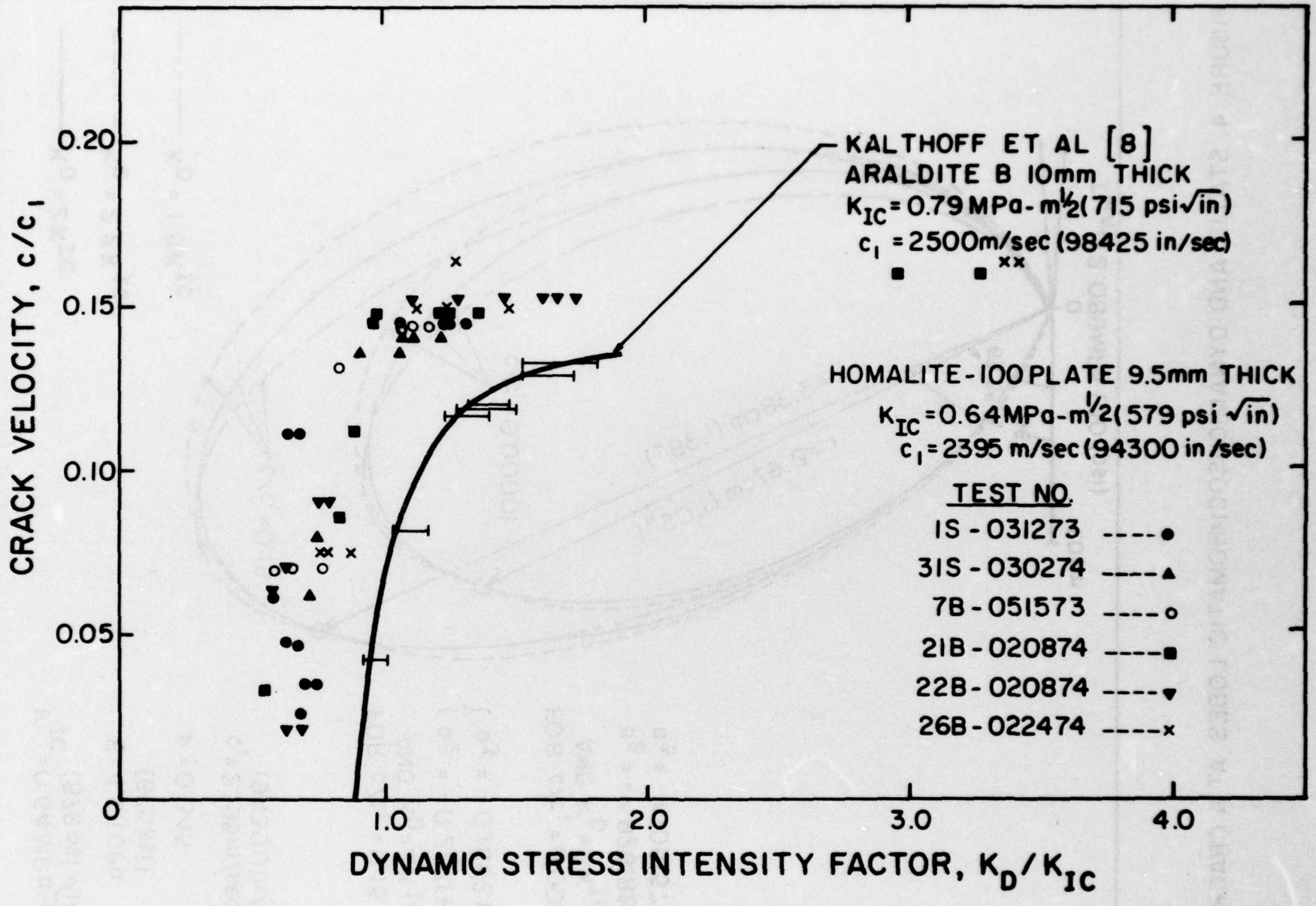

FIGURE 3. SMOOTHED CRACK VELOCITY VERSUS DYNAMIC STRESS INTENSITY FACTOR RELATIONS OF WEDGE-LOADED DCB SPECIMENS.

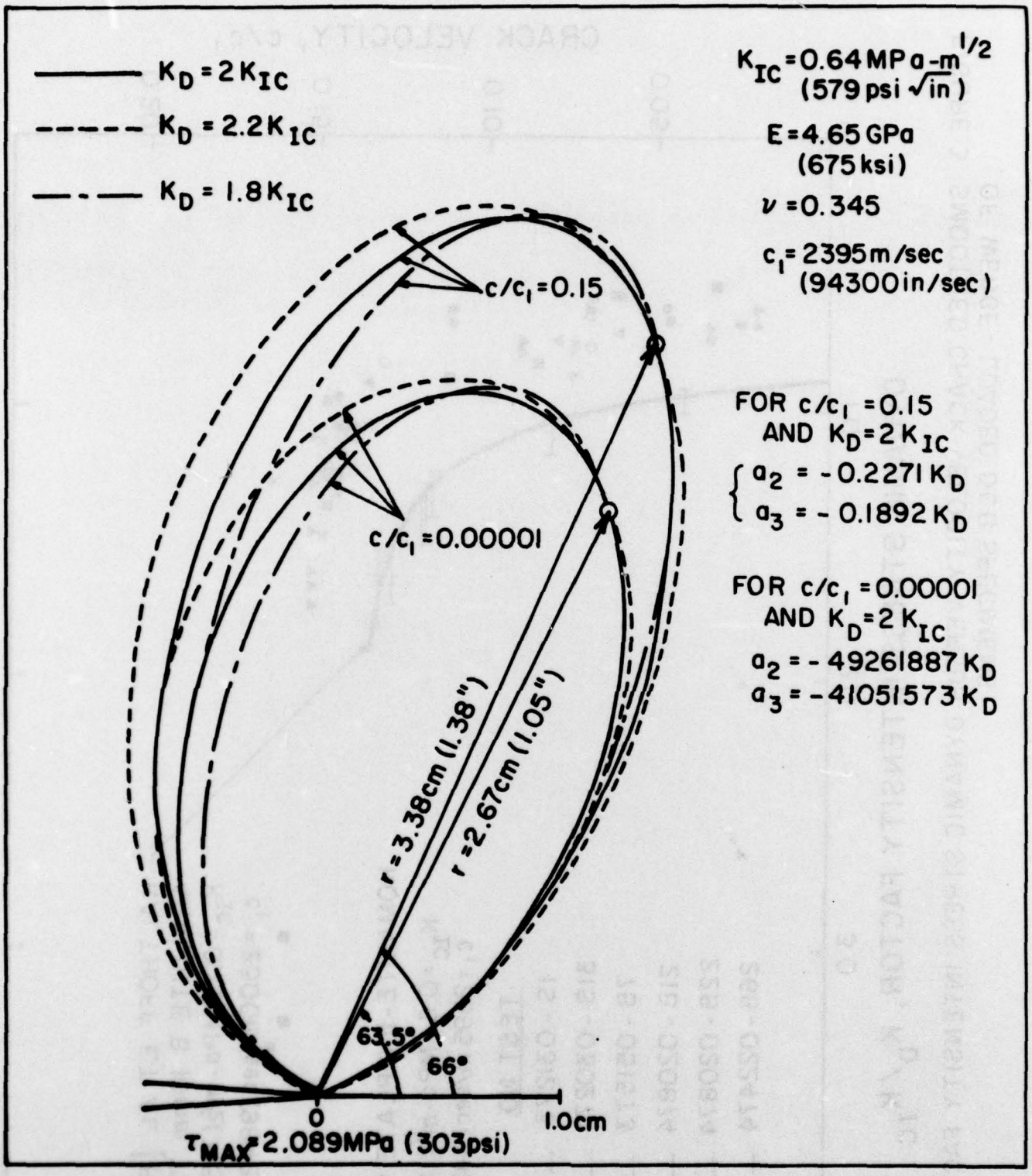

FIGURE 4. STATIC AND DYNAMIC ISOCHROMATIC LOBES AT A CRACK TIP.

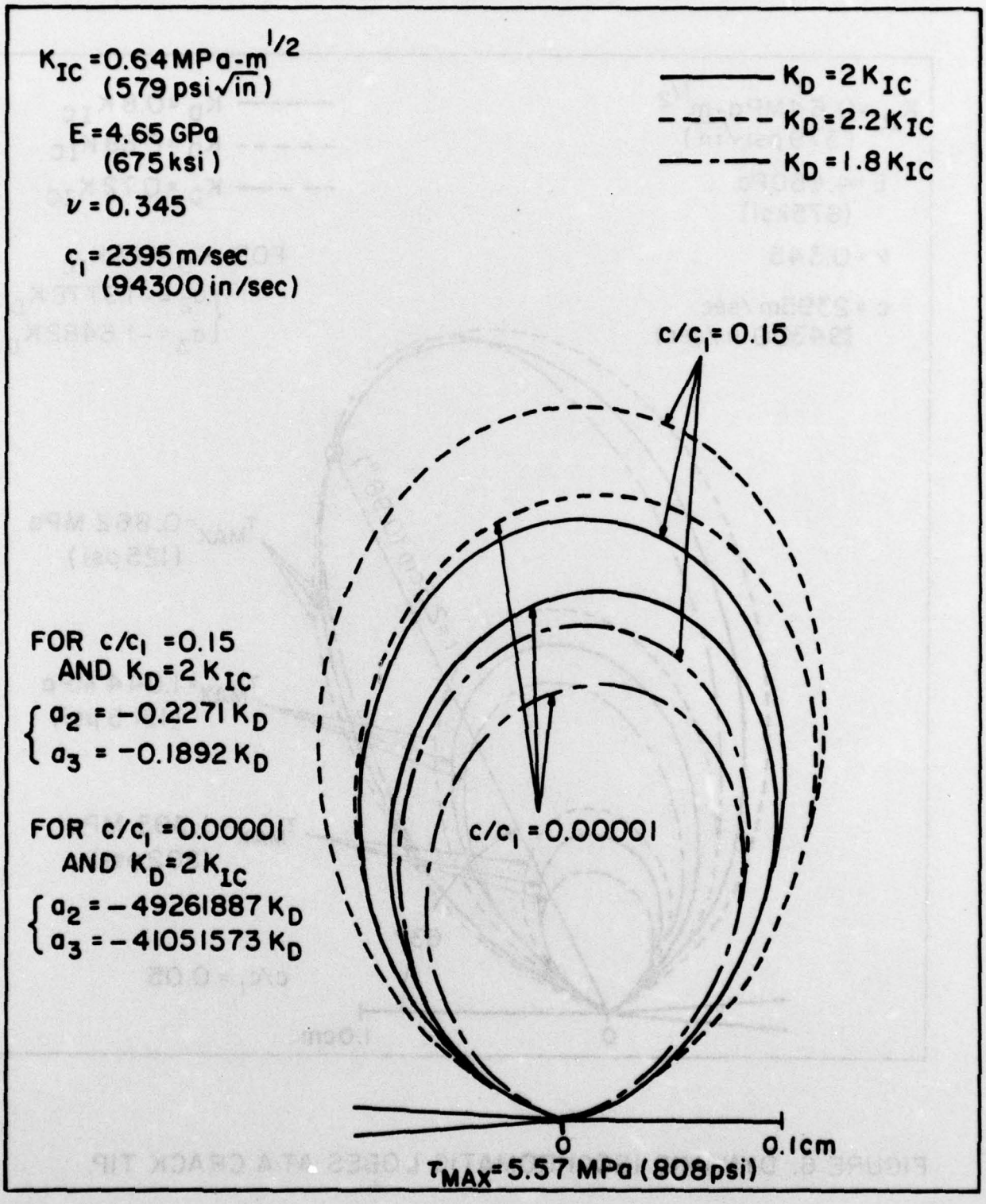

FIGURE 5. STATIC AND DYNAMIC ISOCHOMATIC LOBES AT A CRACK TIP.

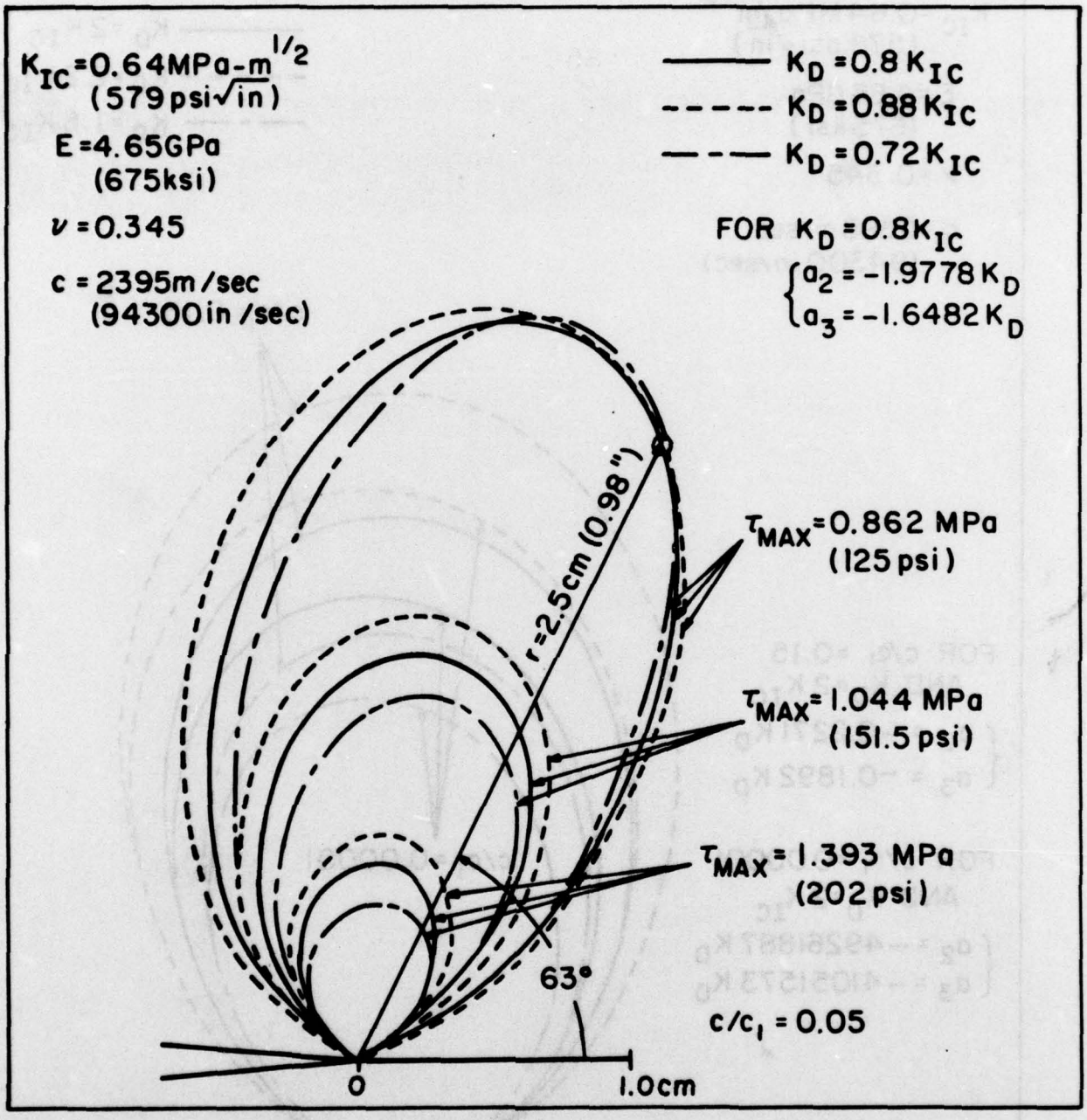

FIGURE 6. DYNAMIC ISOCHROMATIC LOBES AT A CRACK TIP.

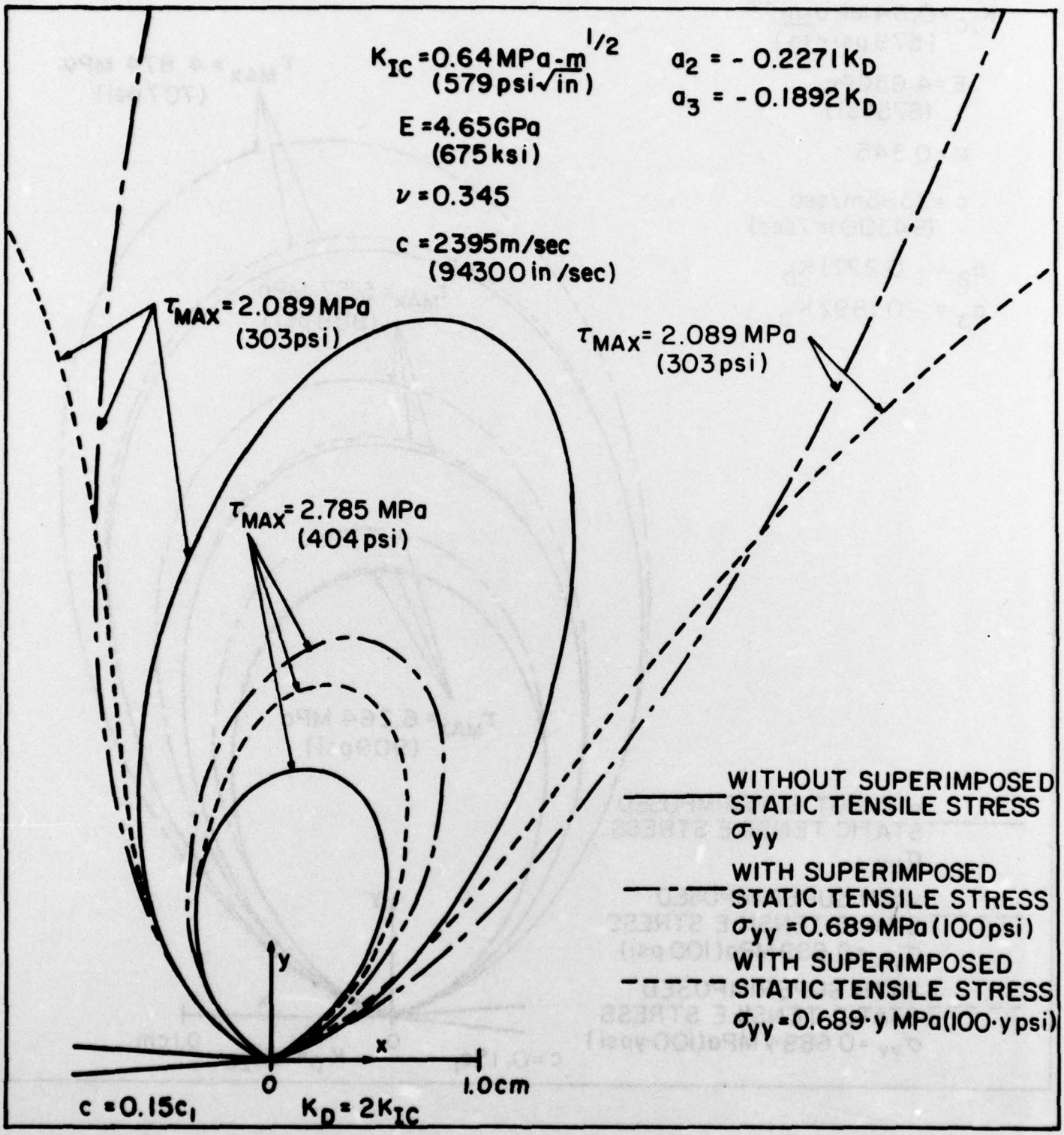

FIGURE 7. DYNAMIC ISOCHROMATIC LOBES AT A CRACK TIP WITH SUPERIMPOSED STATIC TENSILE STRESS σ_{yy}.

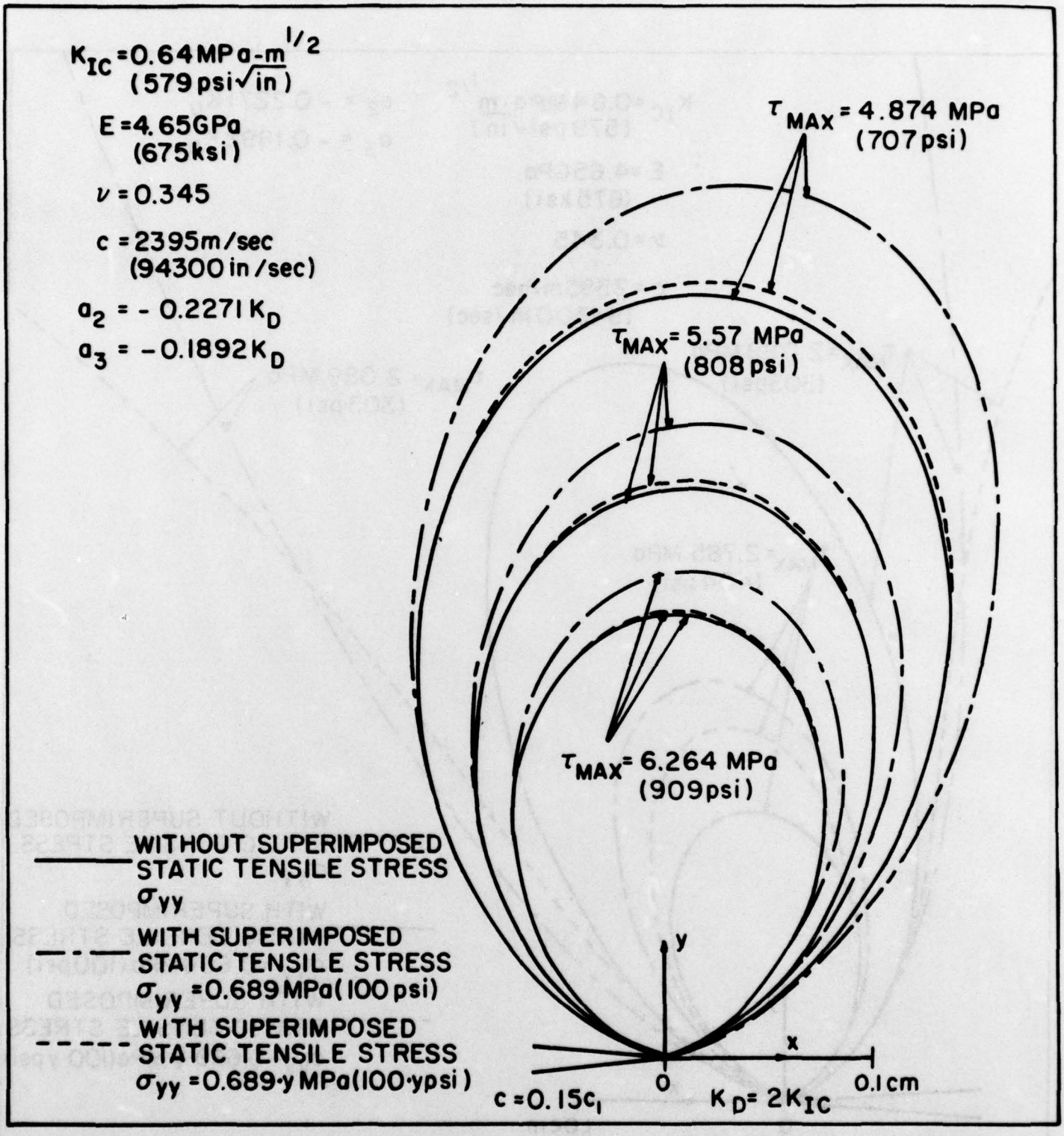

FIGURE 8, DYNAMIC ISOCHROMATIC LOBES AT A CRACK TIP WITH SUPERIMPOSED STATIC TENSILE STRESS σ_{yy}.

Administrative & Liaison Activities

Chief of Naval Research
Department of the Navy
Arlington, Virginia 22217
  Attn: Code 474 (2)
        471
        222

Director
ONR Branch Office
495 Summer Street
Boston, Massachusetts 02210

Director
Naval Research Laboratory
Attn: Code 2629 (ONRL)
Washington, D.C. 20390 (6)

U.S. Naval Research Laboratory
Attn: Code 2627
Washington, D.C. 20390

Director
ONR - New York Area Office
715 Broadway - 5th Floor
New York, N.Y. 10003

Director
ONR Branch Office
1030 E. Green Street
Pasadena, California 91101

Defense Documentation Center
Cameron Station
Alexandria, Virginia 22314 (12)

Army

Commanding Officer
U.S. Army Research Office Durham
Attn: Mr. J.J. Murray
CRD-AA-IP
Box CM, Duke Station
Durham, North Carolina 27706 (2)

Commanding Officer
AMXMR-ATL
Attn: Mr. R. Shea
US Army Materials Res. Agency
Watertown, Massachusetts 02172

Watervliet Arsenal
MAGGS Research Center
Watervliet, New York 12189
  Attn: Director of Research

Technical Library

Redstone Scientific Info. Center
Chief, Document Section
U.S. Army Missile Command
Redstone, Arsenal, Alabama 35809

Army R&D Center
Fort Belvoir, Virginia 22060

Navy

Commanding Officer and Director
Naval Ship Research & Development Center
Bethesda, Maryland 20034
  Attn: Code 042 (Tech. Lib. Br.)
        17
        172
        174
        177
        1800 (Appl. Math. Lab.)
        54125 (Dr. W.D. Sette)
        19
        1901 (Dr. M. Strassberg)
        1945
        196
        1962

Naval Weapons Laboratory
Dahlgren, Virginia 22448

Naval Research Laboratory
Washington, D.C. 20375
  Attn: Code 8400
        8410
        8430
        8440
        6300
        6390
        6380

Undersea Explosion Research Div.
Naval Ship R&D Center
Norfolk Naval Shipyard
Portsmouth, Virginia 23709
  Attn: Dr. E. Palmer
        Code 780

Naval Ship Research & Development Center
Annapolis Division
Annapolis, Maryland 21402
  Attn: Code 2740 - Dr. Y.F. Wang
        28 - Mr. R.J. Wolfe
        281 - Mr. R.B. Niederberger
        2814 - Dr. H. Vandervoldt

Technical Library
Naval Underwater Weapons Center
Pasadena Annex
3202 E. Foothill Blvd.
Pasadena, California 91107

U.S. Naval Weapons Center
China Lake, California 93557
  Attn: Code 4062 - Mr. W. Werback
        4520 - Mr. Ken Bischel

Commanding Officer
U.S. Naval Civil Engr. Lab
Code L31
Port Hueneme, California 93041

Technical Director
U.S. Naval Ordnance Laboratory
White Oak
Silver Spring, Maryland 20910

Technical Director
Naval Undersea R&D Center
San Diego, California 92132

Supervisor of Shipbuilding
U.S. Navy
Newport News, Virginia 23607

Technical Director
Mare Island Naval Shipyard
Vallejo, California 94592

U.S. Navy Underwater Sound Ref. Lab.
Office of Naval Research
PO Box 8337
Orlando, Florida 32806

Chief of Naval Operations
Dept. of the Navy
Washington, D.C. 20350
  Attn: Code Op07T

Strategic Systems Project Office
Department of the Navy
Washington, D.C. 20390
  Attn: NSP-001 Chief Scientist

Deep Submergence Systems
Naval Ship Systems Command
Code 39522
Department of the Navy
Washington, D.C. 20360

Engineering Dept.
US Naval Academy
Annapolis, Maryland 21402

Naval Air Systems Command
Dept. of the Navy
Washington, D.C. 20360
  Attn: NAVAIR 5302 Aero & Structures
        5308 Structures
        52031F Materials
        604 Tech. Library
        320B Structures

Director, Aero Mechanics
Naval Air Development Center
Johnsville
Warminster, Pennsylvania 18974

Technical Director
U.S. Naval Undersea R&D Center
San Diego, California 92132

Engineering Department
U.S. Naval Academy
Annapolis, Maryland 21402

Naval Facilities Engineering Command
Dept. of the Navy
Washington, D.C. 20360
  Attn: NAVFAC 03 Research & Development
        04 " "
        14414 Tech. Library

Naval Sea Systems Command
Dept. of the Navy
Washington, D.C. 20360
  Attn: NAVSHIP 03 Res. & Technology
        031 Ch. Scientist for R&D
        03412 Hydromechanics
        037 Ship Silencing Div.
        035 Weapons Dynamics

Naval Ship Engineering Center
Prince Georges' Plaza
Hyattsville, Maryland 20782
  Attn: NAVSEC 6100 Ship Sys. Engr. & Des. Dep.
        6102C Computer-Aided Ship Des.
        6105C
        6110 Ship Concept Design
        6120 Hull Div.
        6120D Hull Div.
        6128 Surface Ship Struct.
        6129 Submarine Struct.

Air Force

Commander WADD
Wright-Patterson Air Force Base
Dayton, Ohio 45433
  Attn: Code WWRMDD
        AFFDL (FDDS)
        Structures Division
        AFLC (MCEEA)

Chief, Applied Mechanics Group
U.S. Air Force Inst. of Tech.
Wright-Patterson Air Force Base
Dayton, Ohio 45433

Chief, Civil Engineering Branch
WLRC, Research Division
Air Force Weapons Laboratory
Kirtland AFB, New Mexico 87117

Air Force Office of Scientific Research
1400 Wilson Blvd.
Arlington, Virginia 22209
  Attn: Mechanics Div.

NASA

Structures Research Division
National Aeronautics & Space Admin.
Langley Research Center
Langley Station
Hampton, Virginia 23365

National Aeronautic & Space Admin.
Associate Administrator for Advanced
  Research & Technology
Washington, D.C. 02546

Scientific & Tech. Info. Facility
NASA Representative (S-AK/DL)
P.O. Box 5700
Bethesda, Maryland 20014

Other Government Activities

Commandant
Chief, Testing & Development Div.
U.S. Coast Guard
1300 E. Street N.W.
Washington, D.C. 20226

Technical Director
Marine Corps Dev. & Educ. Command
Quantico, Virginia 22134

Director
National Bureau of Standards
Washington, D.C. 20234
  Attn: Mr. B.L. Wilson, EM 219

Dr. M. Gaus
National Science Foundation
Engineering Division
Washington, D.C. 20550

Science & Tech. Division
Library of Congress
Washington, D.C. 20540

Director
Defense Nuclear Agency
Washington, D.C. 20305
  Attn: SPSS

Commander Field Command
Defense Nuclear Agency
Sandia Base
Albuquerque, New Mexico 87115

Director Defense Research & Engrg.
Technical Library
Room 3C-128
The Pentagon
Washington, D.C. 20301

Chief, Airframe & Equipment Branch
FS-120
Office of Flight Standards
Federal Aviation Agency
Washington, D.C. 20553

Chief, Research and Development
Maritime Administration
Washington, D.C. 20235

Deputy Chief, Office of Ship Constrt.
Maritime Administration
Washington, D.C. 20235
  Attn: Mr. U.L. Russo

Atomic Energy Commission
Div. of Reactor Devel. & Tech.
Germantown, Maryland 20767

Ship Hull Research Committee
National Research Council
National Academy of Sciences
2101 Constitution Avenue
Washington, D.C. 20418
  Attn: Mr. A.R. Lytle

PART 2 - CONTRACTORS AND OTHER TECHNICAL COLLABORATORS

Universities

Dr. J. Tinsley Oden
University of Texas at Austin
345 Eng. Science Bldg.
Austin, Texas 78712

Prof. Julius Miklowitz
California Institute of Technology
Div. of Engineering & Applied Sciences
Pasadena, California 91109

Dr. Harold Liebowitz, Dean
School of Engr. & Applied Science
George Washington University
725 23rd St. N.W.
Washington, D.C. 20006

Prof. Eli Sternberg
California Institute of Technology
Div. of Engr. & Applied Sciences
Pasadena, California 91109

Prof. Paul M. Naghdi
University of California
Div. of Applied Mechanics
Etcheverry Hall
Berkeley, California 94720

Professor P.S. Symonds
Brown University
Division of Engineering
Providence, R.I. 02912

Prof. A.J. Durelli
The Catholic University of America
Civil/Mechanical Engineering
Washington, D.C. 20017

Prof. N.J. Tosta
Columbia University
Dept. of Civil Engineering
S.W. Mudd Bldg.
New York, N.Y. 10027

Prof. H.H. Bleich
Columbia University
Dept. of Civil Engineering
Amsterdam & 120th St.
New York, N.Y. 10027

Prof. F.L. DiMaggio
Columbia University
Dept. of Civil Engineering
616 Mudd Building
New York, N.Y. 10027

Prof. A.N. Froudenthal
George Washington University
School of Engineering & Applied Science
Washington, D.C. 20006

D.C. Evans
University of Utah
Computer Science Division
Salt Lake City, Utah 84112

Prof. Norman Jones
Massachusetts Inst. of Technology
Dept. of Naval Architecture & Marine Engineering
Cambridge, Massachusetts 02139

Professor Albert I. King
Biomechanics Research Center
Wayne State University
Detroit, Michigan 48202

Dr. V.R. Hodgson
Wayne State University
School of Medicine
Detroit, Michigan 48202

Dean B.A. Boley
Northwestern University
Technological Institute
2145 Sheridan Road
Evanston, Illinois 60201

Prof. P.G. Hodge, Jr.
University of Minnesota
Dept. of Aerospace Engr. & Mechanics
Minneapolis, Minnesota 55455

Dr. D.C. Drucker
University of Illinois
Dean of Engineering
Urbana, Illinois 61801

Prof. N.M. Newmark
University of Illinois
Dept. of Civil Engineering
Urbana, Illinois 61801

Prof. E. Reissner
University of California, San Diego
Dept. of Applied Mechanics
La Jolla, California 92037

Prof. William A. Nash
University of Massachusetts
Dept. of Mechanics & Aerospace Engr.
Amherst, Massachusetts 01002

Library (Code 0384)
U.S. Naval Postgraduate School
Monterey, California 93940

Prof. Arnold Allentuch
Newark College of Engineering
Dept. of Mechanical Engineering
323 High Street
Newark, New Jersey 07102

Dr. George Herrmann
Stanford University
Dept. of Applied Mechanics
Stanford, California 94305

Prof. J.D. Achenbach
Northwestern University
Dept. of Civil Engineering
Evanston, Illinois 60201

Director, Applied Research Lab.
Pennsylvania State University
P.O. Box 30
State College, Pennsylvania 16801

Prof. Eugen J. Skudrzyk
Pennsylvania State University
Applied Research Laboratory
Dept. of Physics - P.O. Box 30
State College, Pennsylvania 16801

Prof. J. Kempner
Polytechnic Institute of Brooklyn
Dept. of Aero. Engr. & Applied Mech.
333 Jay Street
Brooklyn, N.Y. 11201

Prof. J. Klosner
Polytecnic Institute of Brooklyn
Dept. of Aerospace & Appl. Mech.
333 Jay Street
Brooklyn, N.Y. 11201

Prof. R.A. Schapery
Texas A&M University
Dept. of Civil Engineering
College Station, Texas 77840

Prof. W.D. Pilkey
University of Virginia
Dept. of Aerospace Engineering
Charlottesville, Virginia 22903

Dr. H.G. Schaeffer
University of Maryland
Aerospace Engineering Dept.
College Park, Maryland 20742

Prof. K.D. Willmert
Clarkson College of Technology
Dept. of Mechanical Engineering
Potsdam, N.Y. 13676

Dr. J.A. Stricklin
Texas A&M University
Aerospace Engineering Dept.
College Station, Texas 77843

Dr. L.A. Schmit
University of California, LA
School of Engineering & Applied Science
Los Angeles, California 90024

Dr. M.A. Kamel
The University of Arizona
Aerospace & Mech. Engineering Dept.
Tucson, Arizona 85721

Dr. R.S. Berger
University of Maryland
Dept. of Mechanical Engineering
College Park, Maryland 20742

Prof. G.R. Irwin
Dept. of Mechanical Engineering
University of Maryland
College Park, Maryland 20742

Dr. S.J. Fenves
Carnegie-Mellon University
Dept. of Civil Engineering
Schenley Park
Pittsburgh, Pennsylvania 15213

Dr. Ronald L. Huston
Dept. of Engineering Analysis
Mail Box 112
University of Cincinnati
Cincinnati, Ohio 45221

Prof. George Sih
Dept. of Mechanics
Lehigh University
Bethlehem, Pennsylvania 18015

Prof. A.S. Kobayashi
University of Washington
Dept. of Mechanical Engineering
Seattle, Washington 98195

Librarian
Webb Institute of Naval Architecture
Crescent Beach Road, Glen Cove
Long Island, New York 11542

Prof. Daniel Frederick
Virginia Polytechnic Institute
Dept. of Engineering Mechanics
Blacksburg, Virginia 24061

Prof. A.C. Eringen
Dept. of Aerospace & Mech. Sciences
Princeton University
Princeton, New Jersey 08540

Dr. S.L. Koh
School of Aero., Astro. & Engr. Sci.
Purdue University
Lafayette, Indiana

Prof. E.H. Lee
Div. of Engr. Mechanics
Stanford University
Stanford, California 94305

Prof. R.D. Mindlin
Dept. of Civil Engineering
Columbia University
S.W. Mudd Building
New York, N.Y. 10027

Prof. S.B. Dong
University of California
Dept. of Mechanics
Los Angeles, California 90024

Prof. Burt Paul
University of Pennsylvania
Towne School of Civil & Mech. Engr.
Rm. 113 - Towne Building
220 S. 33rd Street
Philadelphia, Pennsylvania 19104

Prof. H.W. Liu
Dept. of Chemical Engineering & Metall.
Syracuse University
Syracuse, N.Y. 13210

Prof. S. Bodner
Technion R&D Foundation
Haifa, Israel

Prof. R.J.H. Bollard
Chairman, Aeronautical Engr. Dept.
207 Guggenheim Hall
University of Washington
Seattle, Washington 98195

Prof. G.S. Heller
Division of Engineering
Brown University
Providence, Rhode Island 02912

Prof. Werner Goldsmith
Dept. of Mechanical Engineering
Div. of Applied Mechanics
University of California
Berkeley, California 94720

Prof. J.R. Rice
Division of Engineering
Brown University
Providence, Rhode Island 02912

Prof. R.S. Rivlin
Center for the Application of Mathematics
Lehigh University
Bethlehem, Pennsylvania 18015

Library (Code 0384)
U.S. Naval Postgraduate School
Monterey, California 93940

Dr. Francis Cozzarelli
Div. of Interdisciplinary Studies & Research
School of Engineering
State University of New York
Buffalo, N.Y. 14214

Industry and Research Institutes

Library Services Department
Report Section Bldg. 14-14
Argonne National Laboratory
9700 S. Cass Avenue
Argonne, Illinois 60440

Dr. M.C. Junger
Cambridge Acoustical Associates
129 Mount Auburn St.
Cambrige, Massachusetts 02138

Dr. L.H. Chen
General Dynamics Corporation
Electric Boat Division
Groton, Connecticut 06340

Dr. J.E. Greenspon
J.G. Engineering Research Associates
3831 Hamle Drive
Baltimore, Maryland 21215

Dr. S. Ratdorf
The Aerospace Corp.
P.O. Box 92957
Los Angeles, California 90009

Dr. K.C. Park
Lockheed Palo Alto Research Laboratory
Dept. 5233, Bldg. 205
3251 Hanover Street
Palo Alto, California 94304

Library
Newport News Shipbuilding and Dry Dock Co.
Newport New, Virginia 23607

Dr. W.F. Bozich
McDonnell Douglas Corporation
5301 Bolsa Ave.
Huntington Beach, California 92647

Dr. H.N. Abramson
Southwest Research Institute
Technical Vice President
Mechanical Sciences
P.O. Drawer 28510
San Antonio, Texas 78284

Dr. R.C. DeHart
Southwest Research Institute
Dept. of Structural Research
PO Drawer 28510
San Antonio, Texas 78284

Dr. M.L. Baron
Weidlinger Associates,
Consulting Engineers
110 East 59th Street
New York, N.Y. 10022

Dr. W.A. von Riesemann
Sandia Laboratories
Sandia Base
Albuquerque, New Mexico 87115

Dr. T.L. Geers
Lockheed Missiles & Space Co.
Palo Alto Research Laboratory
3251 Hanover Street
Palo Alto, California 94304

Dr. J.L. Tocher
Boeing Computer Services, Inc.
P.O. Box 24346
Seattle, Washington 98124

Mr. William Caywood
Code 3811, Applied Physics Laboratory
8621 Georgia Avenue
Silver Spring, Maryland 20034

Mr. P.C. Durup
Lockheed-California Company
Aeromechanics Dept., 74-43
Burbank, California 91503

Addendum:

Assistant Chief for Technology
Office of Naval Research, Code 200
Arlington, Virginia 22217

Unclassified

SECURITY CLASSIFICATION OF THIS PAGE (When Data Entered)

REPORT DOCUMENTATION PAGE

READ INSTRUCTIONS BEFORE COMPLETING FORM

1. REPORT NUMBER: TR No. 27
2. GOVT ACCESSION NO.:
3. RECIPIENT'S CATALOG NUMBER: (14) TR-27
4. TITLE (and Subtitle): (6) Dynamic Stress Intensity Factor of Homalite-100
5. TYPE OF REPORT & PERIOD COVERED: (9) Interim Report
6. PERFORMING ORG. REPORT NUMBER: 27
7. AUTHOR(s): (10) A.S. Kobayashi [redacted] S. Mall
8. CONTRACT OR GRANT NUMBER(s): (15) N00014-76-C-0060 NR 064-478
9. PERFORMING ORGANIZATION NAME AND ADDRESS: University of Washington, Department of Mechanical Engineering, Seattle, Washington 98195
10. PROGRAM ELEMENT, PROJECT, TASK AREA & WORK UNIT NUMBERS: (12) 25 p.
11. CONTROLLING OFFICE NAME AND ADDRESS: Office of Naval Research, Arlington, Virginia
12. REPORT DATE: (11) Dec [redacted] 76
13. NUMBER OF PAGES: 23
14. MONITORING AGENCY NAME & ADDRESS (if different from Controlling Office):
15. SECURITY CLASS. (of this report):
15a. DECLASSIFICATION/DOWNGRADING SCHEDULE:
16. DISTRIBUTION STATEMENT (of this Report): Unlimited
17. DISTRIBUTION STATEMENT (of the abstract entered in Block 20, if different from Report):
18. SUPPLEMENTARY NOTES:
19. KEY WORDS (Continue on reverse side if necessary and identify by block number): Fracture Mechanics; Impact; Crack Propagation; Dynamic Photoelasticity; Crack Arrest
20. ABSTRACT (Continue on reverse side if necessary and identify by block number):

Dynamic stress intensity factors of Homalite-100 determined by T. Kobayashi and Dally are compared with those previously obtained by the authors where similarities in the two results for single-edged notch specimens of various configurations are noted. Dynamic stress intensity factors of Araldite B obtained by Kalthoff, Beinert and Winkler and those of Homalite-100 obtained by the authors are then compared and again similarities in the two results and in particular the scatters in experimental data for wedge-loaded DCB specimens

(continued on reverse)

DD FORM 1 JAN 73 1473 EDITION OF 1 NOV 65 IS OBSOLETE S/N 0102-014-6601

Unclassified

SECURITY CLASSIFICATION OF THIS PAGE (When Data Entered)

400 344

20. (Continued)

of different sizes are noted. All three teams of investigators used static near-field solution to compute the dynamic stress intensity factors from recorded dynamic isochromatics or dynamic caustics. Errors generated through this use of static near-field solutions as well as through the use of larger isochromatic lobes are thus discussed.